A level-set method for vibration and multiple loads structural optimization

Grégoire ALLAIRE * François JOUVE †

June 23, 2004

Keywords: shape and topology optimization, shape derivative, level-set, eigenfrequency, multiple loads.

Abstract

We extend the level-set method for shape and topology optimization to new objective functions such as eigenfrequencies and multiple loads. This method is based on a combination of the classical shape derivative and of the Osher-Sethian level-set algorithm for front propagation. In two and three space dimensions we maximize the first eigenfrequency or we minimize a weighted sum of compliances associated to different loading configurations. The shape derivative is used as an advection velocity in a Hamilton-Jacobi equation for changing the shape. This level-set method is a low-cost shape capturing algorithm working on a fixed Eulerian mesh and it can easily handle topology changes.

1 Introduction

There are many different numerical methods for the optimal design of elastic structures. The classical method of shape sensitivity (or boundary variation), which is able to perform geometric optimization, has been much studied (see e.g. [25], [30], [33], [35]). The homogenization method (and its variants, such as power-law materials or SIMP method, see e.g. [2], [4], [7], [10], [11], [12], [18]), which can perform topology optimization, is much more recent although it can be more and more considered as classical in view of the number of publications on the subject and available softwares using it. Another method of topology optimization is the so-called bubble method, or topological derivative, proposed by [19], [21], and [34]. Finally there are many evolutionary algorithms (like genetic algorithms) which can be used for topology optimization (see e.g. [23]).

Recently another approach was introduced, based on the use of the level-set method of Osher and Sethian [29], [31] for numerically tracking fronts and free

*Centre de Mathématiques Appliquées (UMR 7641), Ecole Polytechnique, 91128 Palaiseau, France — gregoire.allaire@polytechnique.fr

†Centre de Mathématiques Appliquées (UMR 7641), Ecole Polytechnique, 91128 Palaiseau, France — francois.jouve@polytechnique.fr

boundaries. This level-set method for shape optimization has been developed in [5], [6], [13], [28], [32], [36], [37]. What makes this last method very attractive is that it combines the advantages of the shape sensitivity method and some of those of the homogenization method. Indeed, the level-set method is very general since it can handle any type of objective functions and structural models, including non-linear ones [6], its computational cost is moderate since it is an Eulerian shape capturing method, and it allows for drastic topology changes during the optimization process. However, there still remains one serious drawback: its tendency to fall into local minima far away from global ones (depending on the choice of initial design). This is in sharp contrast with the homogenization method which, being a relaxation method, is insensitive to initialization (see [2] for a discussion of the advantages of relaxation). We do not address this issue of local minima and well-posedness here. Rather, we extend the level-set method as proposed in [5], [6] in two directions. First, we address the maximization of the first eigenfrequency of a structure (see Section 2). Similar problems in the context of a scalar equation (modeling, for example, the vibrations of a membrane) were already addressed in [28]. This is a typical problem in the stiffness maximization of vibrating structures (see e.g. [2], [12]). For example, in civil engineering it is used to design structures less sensitive to low frequency vibrations like earthquakes. The buckling load criterion is very close in practice to the model problem of eigenfrequency maximization that we address here (see, e.g., [20], [26]). Although it is well-known that most algorithms of topology optimization (like homogenization method or SIMP method [2], [10], [12]) are prone to numerical instabilities when maximizing eigenfrequencies (caused by the sudden occurrence of so-called fictitious modes localized in the weak phase mimicking holes), the level set method is surprisingly free from such defaults, which makes it a method of choice for eigenfrequency optimization. Second, we consider multiple loads shape optimization, i.e. we optimize a structure concurrently for several loading configurations (see Section 3). In practice, it amounts to have several state equations and a single objective function that we choose to be a weighted sum of the compliances corresponding to the different forces. It turns out (see e.g. [2], [12]) that a structure which is optimal for several loads (applied separately) is much more stable and safe if the loading conditions are prone to change or are not precisely known.

The main features of our proposed level-set method are a systematic shape differentiation of the objective functions, a front advection using as front velocity the shape derivative, an elasticity analysis on a fixed mesh using the simple "ersatz material" approach (which amounts to fill the holes by a weak phase). Front propagation is performed by solving a Hamilton-Jacobi equation for a level-set function. We put a special emphasis on computational efficiency since we perform 3-d computations which are especially costly. For example, we perform several time steps of the Hamilton-Jacobi transport equation after each elasticity analysis since the former iterations are much faster (being explicit) than the later ones (involving the solution of a large linear system). On the same token, we have implemented a finite element scheme of Abgrall [1] for solving the Hamilton-Jacobi equation on unstructured meshes (which are often used in

industrial applications, see Figure 8.4) where the usual finite difference schemes are unavailable. Section 4 is devoted to the level-set representation of shapes and its advection under the gradient flow of the objective function (this part follows our earlier work [6] but we reproduce it here for the sake of completeness). Section 5 is concerned with the elasticity analysis and the technical details linked to the "ersatz material" approach (many details are new here since there is a delicate interplay between the small rigidity and small density of the weak material mimicking holes). Section 6 describes our optimization algorithm which is a simple gradient method. Finally Section 7 contains our numerical examples in 2 and 3 space dimensions. In particular we exhibit the strong dependence of the computed optimal shape on the initial design. Let us emphasize that our method, based on boundary advection, is not an optimality criteria method like, for example, topological gradient methods [19], [21], [34]. As a consequence, it can safely be analyzed in the framework of gradient methods which guaranties the decrease of the objective function and numerical convergence. Of course, as we already said, it can converge to a local minima, but at least it will not oscillate forever in trying to iteratively solve the optimality condition.

2 Maximizing the first eigenfrequency

We start by describing the eigenvalue problem in linearized elasticity which allows to compute vibration frequencies and modes. Let $\Omega \subset \mathbb{R}^d$ ($d = 2$ or 3) be a bounded open set occupied by a linear isotropic elastic material with Hooke's law A and density $\rho > 0$. Recall that, for any symmetric matrix ξ, A is defined by

$$A\xi = 2\mu\xi + \lambda\big(\mathrm{Tr}\xi\big)\,\mathrm{Id},$$

where μ and λ are the Lamé moduli of the material. The boundary of Ω is made of two disjoint parts

$$\partial\Omega = \Gamma_N \cup \Gamma_D, \tag{2.1}$$

with Dirichlet boundary conditions on Γ_D, and Neumann boundary conditions on Γ_N. The two boundary parts Γ_D and Γ_N are allowed to vary in the optimization process, although it is possible to fix some portion of it (see the numerical examples below).

We denote by $\omega \geq 0$ the vibration frequency and by u the associated mode, i.e. the corresponding displacement field in Ω, which are solution of the eigenvalue problem for the linearized elasticity system

$$\left\{\begin{array}{rcll} -\mathrm{div}\,(A\,e(u)) & = & \omega^2\rho\,u & \text{in } \Omega \\ u & = & 0 & \text{on } \Gamma_D \\ \big(A\,e(u)\big)n & = & 0 & \text{on } \Gamma_N. \end{array}\right. \tag{2.2}$$

As is well known, (2.2) admits a countable infinite family of solutions $(\omega_k, u_k)_{k\geq 1}$ in $\mathbb{R}^+ \times H^1(\Omega)^d$, labeled by increasing order of the eigenfrequency. The eigenfunctions, or modes, are normalized by imposing that $\int_\Omega \rho|u_k|^2 dx = 1$. Furthermore, the first (i.e. smallest) eigenfrequency is characterized as the minimum

value of the Rayleigh quotient, namely

$$\omega_1^2 = \min_{\substack{v\in H^1(\Omega)^d,\, v\neq 0\\ v=0 \text{ on } \Gamma_D}} \frac{\displaystyle\int_\Omega A\, e(v)\cdot e(v)\, dx}{\displaystyle\int_\Omega \rho|v|^2 dx}. \tag{2.3}$$

To emphasize the dependence of the eigenfrequencies on the shape, we shall often denote them by $\omega_k(\Omega)$.

The objective function is denoted by $J(\Omega)$. In rigidity maximization it is common to maximize the first eigenfrequency. Since, by convention, we always minimize the objective function J, we consider

$$J(\Omega) = -\omega_1(\Omega)^2. \tag{2.4}$$

There are many motivations for maximizing the first eigenfrequency. In civil engineering it will make the structure less sensitive to low frequency vibrations like earthquakes. It is very close to the so-called buckling load criterion which is used to test the stability of structures under buckling (see, e.g., [20], [26]). Of course, it is also possible to consider a weighted sum of the k first eigenvalues or any smooth function of them. In particular, it is possible to drive the spectrum of the structure away from some forbidden range of vibration frequencies.

We introduce a working domain D (a bounded open set of $\mathbb{R}^d$) which contains all admissible shapes Ω. We define a set of admissible shapes of fixed volume V

$$\mathcal{U}_{ad} = \Big\{\Omega \subset D \text{ such that } |\Omega| = V\Big\}. \tag{2.5}$$

Our model problem of shape optimization is

$$\inf_{\Omega\in\mathcal{U}_{ad}} J(\Omega). \tag{2.6}$$

Remark 2.1. It is well known that the minimization problem (2.6) is usually not well posed on the set of admissible shapes defined by (2.5) (i.e. it has no solution). In order to obtain existence of optimal shapes, some smoothness or geometrical or topological constraints are required. For example, a variant of (2.6) with a perimeter constraint turns out to be a well-posed problem (see [9]). There are other regularized variants of (2.6) which are well-posed and we refer to [15], [17] for such existence theories. Note that, even if existence is not an issue of the present paper, we shall work with a smoother subset of (2.5), i.e. we consider smooth shapes Ω, in order to define properly a notion of shape derivative.

In order to apply a gradient method to the minimization of (2.6) we recall the classical notion of shape derivative which goes back, at least, to Hadamard (see the modern reference books [30], [35]). Here, we follow the approach of Murat and Simon [25], [33]. Starting from a smooth reference open set Ω, we consider domains of the type

$$\Omega_\theta = \big(\mathrm{Id} + \theta\big)(\Omega),$$

where Id is the identity mapping from $\mathbb{R}^d$ into $\mathbb{R}^d$, and $\theta \in W^{1,\infty}(\mathbb{R}^d, \mathbb{R}^d)$. It is well known that, for sufficiently small θ, $(\mathrm{Id} + \theta)$ is a diffeomorphism in $\mathbb{R}^d$.

Definition 2.2. *The shape derivative of $J(\Omega)$ at Ω is defined as the Fréchet derivative in $W^{1,\infty}(\mathbb{R}^d, \mathbb{R}^d)$ at 0 of the application $\theta \to J\big((\mathrm{Id} + \theta)(\Omega)\big)$, i.e.*

$$J\big((\mathrm{Id} + \theta)(\Omega)\big) = J(\Omega) + J'(\Omega)(\theta) + o(\theta) \quad \textit{with} \quad \lim_{\theta \to 0} \frac{|o(\theta)|}{\|\theta\|} = 0\,,$$

where $J'(\Omega)$ is a continuous linear form on $W^{1,\infty}(\mathbb{R}^d, \mathbb{R}^d)$.

We give two examples of shape derivative that will be useful in the sequel.

Lemma 2.3. *Let Ω be a smooth bounded open set and $\phi(x) \in W^{1,1}(\mathbb{R}^d)$. Define*

$$J_1(\Omega) = \int_\Omega \phi(x)\, dx.$$

Then J_1 is differentiable at Ω and

$$J_1'(\Omega)(\theta) = \int_{\partial\Omega} \theta(x) \cdot n(x)\, \phi(x)\, ds$$

for any $\theta \in W^{1,\infty}(\mathbb{R}^d; \mathbb{R}^d)$. For $\phi(x) \in W^{2,1}(\mathbb{R}^d)$ define

$$J_2(\Omega) = \int_{\partial\Omega} \phi(x)\, ds.$$

Then J_2 is differentiable at Ω and

$$J_2'(\Omega)(\theta) = \int_{\partial\Omega} \theta \cdot n \left(\frac{\partial \phi}{\partial n} + H\phi \right) ds,$$

for any $\theta \in W^{1,\infty}(\mathbb{R}^d; \mathbb{R}^d)$, where H is the mean curvature of $\partial\Omega$ defined by $H = \mathrm{div} n$. Furthermore, this result still holds true if one replaces $\partial\Omega$ by Γ, a smooth open subset of $\partial\Omega$, and assumes that $\phi = 0$ on the surface boundary $\partial\Gamma$.

Remark 2.4. We deduce from Lemma 2.3 the shape derivative of a volume constraint $V(\Omega) = C$ which is

$$V(\Omega) = \int_\Omega dx \quad \text{and} \quad V'(\Omega)(\theta) = \int_{\partial\Omega} \theta(x) \cdot n(x)\, ds.$$

Theorem 2.5. *Let Ω be a smooth bounded open set and $\theta \in W^{1,\infty}(\mathbb{R}^d; \mathbb{R}^d)$. Assume that the first eigenvalue of (2.2) is simple and the associated mode u_1 is smooth, say $u_1 \in H^2(\Omega)^d$. The shape derivative of (2.4) is*

$$\begin{aligned} J'(\Omega)(\theta) \quad &= \frac{\displaystyle\int_{\partial\Omega} \theta \cdot n \Big(\omega^2 \rho\, |u_1|^2 - Ae(u_1) \cdot e(u_1) \Big) ds}{\displaystyle\int_\Omega \rho\, |u_1|^2 dx} \\ &\quad + 2\, \frac{\displaystyle\int_{\Gamma_D} \theta \cdot n\, Ae(u_1) \cdot e(u_1)\, ds}{\displaystyle\int_\Omega \rho\, |u_1|^2 dx}. \end{aligned} \tag{2.7}$$

Remark 2.6. In the numerical examples of Section 7 we shall not optimize the Dirichlet boundary Γ_D which amounts to cancel the last term of (2.7). If the first eigenvalue of (2.2) is not simple, then it is still possible to compute a directional derivative (see e.g. [22], [27]). Of course, a similar result holds for any simple eigenvalue, not necessarily the first one.

Proof. Although Theorem 2.5 is a classical result (see e.g. [16], [25], [30], [33], [35]) we briefly sketch its proof for the sake of completeness. Since the first eigenvalue is assumed to be simple, it is shape-differentiable. To obtain the value of the shape derivative we introduce the Lagrangian defined for any $(v, q) \in H^1(\mathbb{R}^d; \mathbb{R}^d)^2$ by

$$\mathcal{L}(\Omega, v, q) = -\frac{\displaystyle\int_\Omega A\, e(v) \cdot e(v)\, dx - 2\int_{\Gamma_D} q \cdot v\, ds}{\displaystyle\int_\Omega \rho |v|^2 dx} \tag{2.8}$$

where q is a Lagrange multiplier for the Dirichlet boundary condition on Γ_D. It is worth noticing that v and q belong to a functional space that does not depend on Ω, so we can apply the usual differentiation rule to the Lagrangian $\mathcal{L}$. Clearly, for a given open set Ω, $\mathcal{L}$ has a min-max or saddle point (p, u) and

$$J(\Omega) = \max_{v \in H^1(\mathbb{R}^d;\mathbb{R}^d)} \min_{q \in H^1(\mathbb{R}^d;\mathbb{R}^d)} \mathcal{L}(\Omega, v, q)$$

(minimizing first in q we recover the Dirichlet boundary condition for v on Γ_D). Then, u is a solution of (2.2) with eigenvalue ω^2 and we normalize it by

$$\int_\Omega \rho |u|^2 dx = 1.$$

The stationarity of the Lagrangian gives the optimality conditions. The partial derivative of $\mathcal{L}$ with respect to q in the direction $\phi \in H^1(\mathbb{R}^d; \mathbb{R}^d)$ is

$$\langle \frac{\partial \mathcal{L}}{\partial q}(\Omega, u, p), \phi \rangle = 2\int_{\Gamma_D} u \cdot \phi\, ds,$$

which, when it vanishes, implies that $u = 0$ on Γ_D. The partial derivative of $\mathcal{L}$ with respect to v in the direction $\phi \in H^1(\mathbb{R}^d; \mathbb{R}^d)$ is

$$\begin{aligned} \langle \frac{\partial \mathcal{L}}{\partial v}(\Omega, u, p), \phi \rangle \quad &= -2\int_\Omega A\, e(u) \cdot e(\phi)\, dx + 2\int_{\Gamma_D} p \cdot \phi\, ds \\ &\quad +2\int_\Omega \rho v \cdot \phi\, dx \left(\int_\Omega A\, e(u) \cdot e(u)\, dx \right). \end{aligned}$$

Since $\frac{\partial \mathcal{L}}{\partial v}(\Omega, u, p) = 0$, taking first ϕ with compact support in Ω gives, after integration by parts,

$$-\mathrm{div}\,(A\, e(u)) = \left(\int_\Omega A\, e(u) \cdot e(u)\, dx \right) \rho\, u = \omega^2 \rho\, u \quad \text{in } \Omega, \tag{2.9}$$

which is nothing but the state equation (2.2). Then, varying the trace function ϕ on Γ_N gives the Neumann boundary condition, while varying the trace function ϕ on Γ_D gives the value of the Lagrange multiplier $p = A\,e(u)n$.

The shape derivative of the objective function is obtained by differentiating

$$J(\Omega) = \mathcal{L}(\Omega, u(\Omega), p(\Omega)),$$

which, by the chain rule theorem, reduces to the partial derivative of $\mathcal{L}$ with respect to Ω in the direction θ

$$J'(\Omega)(\theta) = \frac{\partial \mathcal{L}}{\partial \Omega}(\Omega, u, p)(\theta).$$

Note that, since the first eigenvalue is simple, the first eigenvector $u(\Omega)$ is shape-differentiable, and so is $p(\Omega) = A\,e(u(\Omega))n$. Applying Lemma 2.3 we obtain

$$\begin{aligned} \frac{\partial \mathcal{L}}{\partial \Omega}(\Omega, u, p)(\theta) = \quad & -\int_{\partial\Omega} Ae(u)\cdot e(u)\,\theta\cdot n\,ds \\ & +2\int_{\Gamma_D} \theta\cdot n\left(\frac{\partial(p\cdot u)}{\partial n} + H\,p\cdot u\right) ds \\ & +\left(\int_\Omega Ae(u)\cdot e(u)\,dx\right)\int_{\partial\Omega}\theta\cdot n\,\rho|u|^2 ds. \end{aligned} \tag{2.10}$$

Taking into account the boundary condition $u = 0$ and $p = A\,e(u)n$ on Γ_D, which also implies $Ae(u)\cdot e(u) = \frac{\partial u}{\partial n}\cdot Ae(u)n$ on Γ_D, we deduce

$$\begin{aligned} \frac{\partial \mathcal{L}}{\partial \Omega}(\Omega, u)(\theta) = \quad & \int_{\partial\Omega}\theta\cdot n\Big(\omega^2\rho|u|^2 - Ae(u)\cdot e(u)\Big) ds \\ & +2\int_{\Gamma_D}\theta\cdot n\,Ae(u)\cdot e(u)\,ds, \end{aligned}$$

which yields (2.7) where no adjoint state is involved (thus the minimization of (2.4) is a self-adjoint problem). □

3 Multiple loads optimization

We keep the notations of the previous Section 2. We consider $n \geq 1$ possible loading configurations for a structure Ω, indexed by i: f_i is the vector-valued function of the volume forces and g_i that of the surface loads. The corresponding displacement field u_i in Ω is the solution of the linearized elasticity system

$$\left\{\begin{array}{rcll} -\mathrm{div}\,(A\,e(u_i)) & = & f_i & \text{in } \Omega \\ u_i & = & 0 & \text{on } \Gamma_D \\ \big(A\,e(u_i)\big)n & = & g_i & \text{on } \Gamma_N. \end{array}\right. \tag{3.1}$$

Since Ω is varying during the optimization process, f_i and g_i must be known for all possible configurations of Ω. Therefore, introducing a working domain

$D \subset \mathbb{R}^d$ which contains all admissible shapes Ω, we take $f_i \in L^2(D)^d$ and $g_i \in H^1(D)^d$. We assume further that the surface measure of Γ_D is not zero (otherwise we should impose an equilibrium condition on f_i and g_i). In such a case it is well known that (3.1) admits a unique solution $u_i \in H^1(\Omega)^d$.

A multiple loads problem is a problem for which the objective function $J(\Omega)$ depends on the n displacement fields u_i. For simplicity, in this paper, we focus on the sum of the compliances, i.e. we consider

$$J(\Omega) = \sum_{i=1}^{n} \left(\int_\Omega f_i \cdot u_i \, dx + \int_{\Gamma_N} g_i \cdot u_i \, ds \right) = \sum_{i=1}^{n} \int_\Omega A\, e(u_i) \cdot e(u_i) \, dx, \quad (3.2)$$

which is very common in rigidity maximization. The single loading case ($n = 1$), as well as various other objective functions, were treated in [6]. Of course, it is easy to introduce arbitrary weights in front of the individual compliances in (3.2) for balancing the loading configurations differently in the objective function. The main practical interest of multiple loads shape optimization is to obtain stable structures. Indeed, an optimal shape for a single load may be so optimal that it is unstable (or at least too compliant) for any other applied load. Therefore, an optimal shape for multiple loads is much more safe if the loading conditions are not precisely known or subject to change.

Recalling definition (2.5) of the set $\mathcal{U}_{ad}$ of admissible shapes, our model problem of multiple loads shape optimization is

$$\inf_{\Omega \in \mathcal{U}_{ad}} J(\Omega).$$

The shape derivative of (3.2) is easily obtained by summing the shape derivatives of the single load compliances.

Theorem 3.1. *Let Ω be a smooth bounded open set and $\theta \in W^{1,\infty}(\mathbb{R}^d;\mathbb{R}^d)$. Assume that the data f_i and g_i as well as the solutions u_i of (3.1) are smooth, say $f_i \in H^1(\Omega)^d$, $g_i \in H^2(\Omega)^d$, $u_i \in H^2(\Omega)^d$. The shape derivative of (3.2) is*

$$\begin{aligned} J'(\Omega)(\theta) = \sum_{i=1}^{n} \Bigg(& \int_{\Gamma_N} \left(2 \left[\frac{\partial (g_i \cdot u_i)}{\partial n} + H g_i \cdot u_i + f_i \cdot u_i \right] - A e(u_i) \cdot e(u_i) \right) \theta \cdot n \, ds \\ & + \int_{\Gamma_D} A e(u_i) \cdot e(u_i)\, \theta \cdot n \, ds \Bigg). \end{aligned} \quad (3.3)$$

For a proof of Theorem 3.1 we refer to [6] in the single load case or to the classical works [25], [30], [33], [35]. There is no adjoint state involved in (3.3). Indeed the minimization of (3.2) is a self-adjoint problem.

Remark 3.2. Very often the adequate set of weights to put in front of the compliances in the summed objective function (3.2) for properly balancing the loading configurations is unknown and difficult to find numerically. Therefore, a common choice is to replace (3.2) by the new objective function

$$J(\Omega) = \max_{1 \le i \le n} \left(c_i(\Omega) = \int_\Omega f_i \cdot u_i \, dx + \int_{\Gamma_N} g_i \cdot u_i \, ds \right).$$

Since the maximum function is not differentiable, the shape optimization problem is then rewritten as

$$\inf_{\substack{\Omega\in\mathcal{U}_{ad},\beta\in\mathbb{R}\\ c_i(\Omega)\le\beta,\ 1\le i\le n}} \beta$$

which is a smooth constrained minimization. We do not know if the level-set method can also be applied successfully to this objective function. In numerical practice we used only the objective function (3.2) so far.

4 Shape representation by the level-set method

From the previous sections we have all the necessary theoretical ingredients to introduce a gradient method for the minimization of an objective function $J(\Omega)$. The general form of its shape derivative is

$$J'(\Omega)(\theta) = \int_{\partial\Omega} v\,\theta\cdot n\,ds,$$

where the function v is given by a result like Theorem 2.5 or Theorem 3.1. Ignoring smoothness issues, a descent direction is found by defining a vector field

$$\theta = -v\,n, \tag{4.1}$$

and then we update the shape Ω as

$$\Omega_t = (\,\mathrm{Id} + t\theta)\Omega,$$

where $t>0$ is a small descent step. Formally, we obtain

$$J(\Omega_t) = J(\Omega) - t\int_{\partial\Omega} v^2\,ds + \mathcal{O}(t^2)$$

which guarantees the decrease of the objective function.

Remark 4.1. There are other possible choices for the definition of the descent direction. Let us first remark that, from a mathematical point of view, formula (4.1) makes sense only if the resulting vector field θ is smooth enough, i.e. belongs to $W^{1,\infty}(\mathbb{R}^d,\mathbb{R}^d)$. If either v or the normal n is not smooth, then it may be desirable to smooth the velocity field vn (this is a classical issue in shape optimization ; see e.g. [8], [13], Chapter 5 in [24]). We refer to the above references for more details. Our numerical experience shows that the simple choice (4.1) is enough in practice.

As just described, the method of shape sensitivity can be (and has been) implemented in a Lagrangian framework. It suffices to mesh Ω and to advect the mesh according to the descent direction θ. However, this implementation suffers at least from two drawbacks. First, if the shape is deformed too much, then it is necessary to remesh which can be very costly (especially in 3-d). Second, different parts of the boundary of the shape may want to merge or

split, but as is well known topology changes are very difficult to handle with such Lagrangian or front-tracking methods. Therefore, we favor an Eulerian approach and we use a level-set method to capture the shape Ω on a fixed mesh.

The level-set method is versatile and computationally very efficient: it is by now a classical tool in many fields such as motion by mean curvature, fluid mechanics, image processing, etc. Let us describe simply how it works. Let a bounded domain $D \subset \mathbb{R}^d$ be the working domain in which all admissible shapes Ω are included, i.e. $\Omega \subset D$. In numerical practice, the domain D will be meshed once and for all. We parametrize the boundary of Ω by means of a level-set function, following the idea of Osher and Sethian [29]. We define this level-set function ψ in D such that

$$\begin{cases} \psi(x) = 0 & \Leftrightarrow x \in \partial\Omega \cap D, \\ \psi(x) < 0 & \Leftrightarrow x \in \Omega, \\ \psi(x) > 0 & \Leftrightarrow x \in \left(D \setminus \overline{\Omega}\right). \end{cases}$$

The normal n to the shape Ω is recovered as $\nabla\psi/|\nabla\psi|$ and the curvature H is given by the divergence of the normal div$n$ (these quantities are evaluated by finite differences when the mesh is uniformly rectangular). Remark that, although n and H are theoretically defined only on $\partial\Omega$, the level-set method allows to define easily their extension in the whole domain D (this will be useful in the sequel).

Following the optimization process, the shape is going to evolve according to a fictitious time which corresponds to descent stepping. As is well-known, if the shape is evolving in time, then the evolution of the level-set function is governed by a simple Hamilton-Jacobi equation. To be precise, assume that the shape $\Omega(t)$ evolves in time $t \in \mathbb{R}^+$ with the normal velocity $-v(t,x)n$ as proposed in (4.1). Then

$$\psi\Big(t, x(t)\Big) = 0 \quad \text{for any } x(t) \in \partial\Omega(t).$$

Differentiating in t yields

$$\frac{\partial\psi}{\partial t} + \dot{x}(t) \cdot \nabla\psi = \frac{\partial\psi}{\partial t} - vn \cdot \nabla\psi = 0.$$

Since $n = \nabla\psi/|\nabla\psi|$ we obtain

$$\frac{\partial\psi}{\partial t} - v|\nabla\psi| = 0. \tag{4.2}$$

This Hamilton-Jacobi equation is posed in the whole box D, and not only on the boundary $\partial\Omega$, if the velocity v is known everywhere (as will be the case in the sequel). Transporting ψ by (4.2) is equivalent to move the boundary of Ω (the zero level-set of ψ) along the descent gradient direction $-J'(\Omega)$.

Boundary conditions on ∂D must be added to the Hamilton-Jacobi equation (4.2). Our choice, which is the most common one, is to consider Neumann boundary conditions

$$\frac{\partial\psi}{\partial n} = 0 \quad \text{on } \partial D.$$

It has many advantages and one drawback. First, it is easy to implement since there is no reference value to assign for ψ at the boundary. Second, it implies that the solution of (4.2) satisfies a maximum principle. More precisely, new holes in Ω can appear only by advecting the zero level-set of ψ which changes its topology and can not come from outside the domain D because of spurious values created by the boundary conditions. The drawback is that the Neumann boundary condition makes the level sets of ψ orthogonal to the boundary which is not always the best geometric configuration for minimizing the objective function. We tried other types of boundary condition but none of them was fully successful mainly because it yields spurious holes appearing at the boundary.

One can wonder why it is better to solve the non-linear Hamilton-Jacobi equation (4.2) rather than the simpler linear transport equation

$$\frac{\partial \psi}{\partial t} - v\, n \cdot \nabla \psi = 0, \tag{4.3}$$

where n as v would be given by the previous shape in an iterative scheme. The main reason is that (4.2) is somehow more robust than its linear counterpart for large times. Indeed, the solution of (4.2) is guaranteed to advance along its normal *at all times*, while the solution of the linear equation (4.3) is advected along the normal of the initial level-set function. If we were to make only one small time step of (4.2), then there would be not so much difference between the linear and the non-linear equations. However, in most cases we shall perform of the order of 10 to 50 time steps of (4.2) for each evaluation of the normal velocity v. Therefore, the non-linear equation (4.2) gives much better results.

The Hamilton-Jacobi equation (4.2), being non-linear, does not admit smooth solutions. However, it admits a unique viscosity solution (or weak solution) which properly defines a generalized shape evolution. In order to capture this viscosity solution, (4.2) must be solved by an upwind scheme [29], [31]. Note that, although the notion of viscosity solutions is the proper one for computing the physically relevant solution in many problems (such as fronts propagating under their mean curvature), it is not clear that it is the best possible choice for shape optimization. Indeed, the shape derivative obtained in Theorems 2.5 or 3.1 is valid as long as the shape is smooth. On the other hand, viscosity solutions depart from smooth solutions (or other possible types of solutions) precisely when the shape starts to be non-smooth (i.e. to have corner or cusps).

In practice we use a simple second order explicit upwind scheme (see e.g. [31]) on Cartesian grids, and a more delicate explicit first order upwind scheme (see [1]) for non-structured meshes. Since these schemes are explicit in time, their time stepping must satisfy a CFL condition. Usually the time step issued from this CFL condition is much smaller than the time step Δt_k which plays the role of the descent step in the minimization of $J(\Omega)$. Of course, one explicit time step for (4.2) is much cheaper, in terms of CPU time and memory requirement, than the solution of the state equation (2.2) or (3.1).

Because of its advection or because of numerical diffusion the level-set function may become too flat or too steep which yields either large errors in the

location of its zero level set or large errors in the evaluation of its gradient by finite differences (which in turn implies a bad approximation of the normal n or of the curvature H). Therefore, it is usual to regularize it periodically by solving the following problem

$$\left\{ \begin{array}{rcll} \dfrac{\partial \psi}{\partial t} + \mathrm{sign}(\psi_0)\Big(|\nabla \psi| - 1\Big) & = & 0 & \text{in } D \times \mathbb{R}^+, \\ \psi(t=0,x) & = & \psi_0(x) & \text{in } D, \end{array} \right. \tag{4.4}$$

which admits as a stationary solution the signed distance to the initial interface $\{\psi_0(x) = 0\}$.

5 Elasticity analysis of the structure

The elasticity equations for the state u (or u_i, $1 \leq i \leq n$ in the multiple loads case) are extended to the whole domain D by using the so-called "ersatz material" approach. It amounts to fill the holes $D \backslash \Omega$ by a weak phase mimicking void but avoiding the singularity of the rigidity matrix. This is a well-known procedure in topology optimization which can be rigorously justified in some cases [2]. More precisely, as in [6] we define an elasticity tensor $A^*(x)$ which s a mixture of A in Ω and of the weak material mimicking holes in $D \setminus \Omega$

$$A^*(x) = h(x)A \quad \text{with} \quad h = \left\{ \begin{array}{ll} 1 & \text{in } \Omega, \\ h_{min} & \text{in } D \setminus \Omega. \end{array} \right. \tag{5.1}$$

Compared to our previous work [6], we also need to apply the same procedure for the material density (required for the eigenfrequency problem (2.2)) by introducing a mixture density

$$\rho^*(x) = \tilde{h}(x)\rho \quad \text{with} \quad \tilde{h} = \left\{ \begin{array}{ll} 1 & \text{in } \Omega, \\ \tilde{h}_{min} & \text{in } D \setminus \Omega. \end{array} \right. \tag{5.2}$$

In numerical practice, $h(x)$ and $\tilde{h}(x)$ are piecewise constant in each cell and adequately interpolated in the cells cut by the shape boundary (the zero level-set $\psi = 0$). Unlike the homogenization method or any other generalized material method, the interpolated functions h and $\tilde{h}$ in (5.1), (5.2) are always equal to their extreme values except in a thin zone around the shape boundary which *does not increase in thickness* during the optimization process. For eigenfrequency optimization the correct choice of the threshold parameters is always delicate since a bad combination can yield spurious eigenmodes localized in the ersatz material. We found that a convenient choice of the threshold parameters is

$$h_{min} = 10^{-2} \quad \text{and} \quad \tilde{h}_{min} = 10^{-4},$$

while for multiple loads optimization we usually take $h_{min} = 10^{-3}$.

To be more specific, let us consider the approximation of the eigenvalue problem (2.2) (the case of the multiple loads equation (3.1) is similar to that

exposed in our previous work [6]). The boundary ∂D of the working domain is decomposed in two parts

$$\partial D = \partial D_D \cup \partial D_N,$$

such that ∂D_D corresponds to Dirichlet boundary conditions, and ∂D_N to homogeneous Neumann boundary conditions (traction-free). Recall the decomposition (2.1) of the shape boundary, $\partial\Omega = \Gamma_D \cup \Gamma_N$. Admissible shapes Ω are further constrained to satisfy

$$\Gamma_D \subset \partial D_D, \quad \Gamma_N \cap \partial D_D = \emptyset. \tag{5.3}$$

In other words, the boundary Γ_D, with zero displacement, must be a subset of the fixed boundary ∂D_D, while the traction-free boundary Γ_N can be anywhere but on ∂D_D. Consequently, the only optimized part of the shape boundary is Γ_N which is traction free. These conditions are precisely those assumed in all numerical examples of Section 7. Then, the displacement u is computed as the solution of

$$\left\{ \begin{array}{rcll} -\mathrm{div}\,(A^*\, e(u)) & = & \omega^2 \rho^* u & \text{in } D \\ u & = & 0 & \text{on } \partial D_D \\ \big(A^* e(u)\big) n & = & 0 & \text{on } \partial D_N. \end{array} \right. \tag{5.4}$$

The homogeneous Neumann boundary condition on the interior part of Γ_N (i.e. that part which does lie on ∂D_N) is automatically taken into account in the weak formulation of (5.4), at least in the limit when the rigidity h_{min} of the ersatz material goes to zero.

Remark 5.1. In order to get non-trivial shapes when maximizing the first eigenfrequency, we shall always impose that the admissible shapes Ω include a fixed zone which is not subject to optimization and which is usually heavier. Typically, the material density in these fixed subregions is 10 to 100 times larger than the current value of ρ.

6 Optimization algorithm

For the minimization problem

$$\inf_{\Omega \in \mathcal{U}_{ad}} J(\Omega),$$

we computed a shape derivative

$$J'(\Omega)(\theta) = \int_{\partial\Omega} v\, \theta \cdot n \, ds,$$

where the scalar function v is given by Theorems 2.5 or 3.1. A key point is that, since n and H, as well as the state u or u_i, are computed everywhere in D, the integrand v in the shape derivative is defined throughout the domain D and not only on the free boundary $\partial\Omega$.

Our algorithm, as proposed in [6], is an iterative method, structured as follows:

1. Initialization of the level-set function ψ_0 corresponding to an initial guess Ω_0. Typically, Ω_0 is the full domain D perforated by a periodic distributions of circular holes.

2. Iteration until convergence, for $k \geq 0$:

   (a) Computation of the state u_k by solving a linear elasticity problem in Ω_k, approximated by (5.4) for eigenfrequency optimization or by a similar regularization in the multiple loads case (see [6] for details).

   (b) Deformation of the shape by solving the transport Hamilton-Jacobi equation (4.2). The new shape Ω_{k+1} is characterized by the level-set function ψ_{k+1} solution of (4.2) after a time step Δt_k starting from the initial condition $\psi_k(x)$ with velocity $-v_k$ computed in terms of u_k. The time step Δt_k is chosen such that $J(\Omega_{k+1}) \leq J(\Omega_k)$.

3. From time to time, for stability reasons, we also reinitialize the level-set function ψ by solving (4.4).

The time step Δt_k is monitored by the decrease of the objective function. Typically, we increase Δt_k (up to some given upper limit) when J decreases, while we reduce Δt_k and go back to the previous iteration if J increases. Usually, for each iteration k in the above algorithm (corresponding to a single evaluation of the elastic displacement u_k), we perform several (from 10 to 50) explicit time steps of the Hamilton-Jacobi equation (4.2).

Remark 6.1. One of the main advantages of the level-set method is that we never have to know where precisely is the boundary $\partial\Omega$. In particular, the same numerical scheme for solving the Hamilton-Jacobi equation (4.2) is applied everywhere in the working domain D.

Remark 6.2. The level-set method is well known to handle easily topology changes, i.e. merging or cancellation of holes. Therefore, the above algorithm is able to perform topology optimization. In 2-d our algorithm does not create new holes or boundaries, at least if the Hamilton-Jacobi equation (4.2) is solved under a strict CFL condition. Indeed, a new hole can not nucleate right in the middle of a material zone because (4.2) satisfies a maximum principle. The only possible mechanism is that an initial hole splits in two new holes, which is usually very unlikely when stiffness is maximized. The 3-d case is very different since there are less topological constraints for the creation of new holes. Numerical practice suggest that the initial topology is less important in 3-d than in 2-d.

7 Numerical results for eigenfrequency maximization

In all computations we use a regular quadrangular mesh for both the level-set function and the elastic displacement. We use $Q1$ finite elements for the elasticity analysis. All test cases have the following data, unless otherwise specified.

The Young modulus E of material A is normalized to 1, the Poisson ratio ν is fixed to 0.3 and the material density is set to 1. The void or holes are mimicked by an ersatz material with the same Poisson ratio, a smaller Young modulus by a factor of 10^{-2} and a smaller density by a factor of 10^{-4}. Although this "ersatz material approach", used within the framework of homogenization or SIMP methods, is known to produce fictitious eigenmodes, localized in the weak phase, which pollutes the optimization process (see e.g. [2], [10], [12]), we did not encounter any numerical problem of this type with the level set method when a strict decrease of the objective function is required at each gradient step. We believe this is due to the fact that small holes or material islands can not suddenly appear or disappear between two successive iterations with the level-set method as they do with the homogenization or SIMP methods. In this regard, the level-set method is especially well suited for eigenfrequency optimization.

For each elasticity analysis (that we call iteration in the sequel) we perform 20 explicit time steps of the second-order scheme for the Hamilton-Jacobi transport equation. We also reinitialize the level-set function every 5 time steps of transport by performing 5 explicit time steps of equation (4.4).

Our gradient method is valid only if the first eigenvalue is simple, which ensures its differentiability. In the case of a multiple first eigenvalue (which is usually not differentiable but merely admits directional derivatives), one should resort to a subgradient type algorithm as proposed e.g. in [22], [27]. We checked that, for all test cases presented here, the optimal first eigenvalue is simple, and thus differentiable. In most cases, the first eigenvalue remains simple throughout during the optimization process (see Figure 7.2 right) but on one example an eigenvalue crossing seems to occur (see Figure 7.4 left).

7.1 2-d cantilever

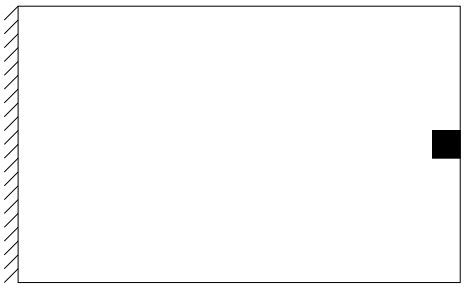

Figure 7.1: Boundary conditions for a 2-d cantilever (the black zone is heavier and not subject to optimization)

In the two-dimensional setting $d = 2$ we first study a medium cantilever problem. The working domain is a rectangle of size 2×1 discretized with a rectangular 80×40 mesh, with zero displacement boundary condition on the left side and a small square region at the middle of the right side (see Figure 7.1)

which is 100 times heavier and is not subject to optimization (no material can be removed in this square). Taking a heavy tip mass is common practice in structural optimization, but to demonstrate the robustness of our algorithm we also consider a tip mass with the same material density in Figure 7.5 (right).

Admissible shapes $\Omega \subset D$ must satisfy the constraint (5.3), i.e.

$$\partial\Omega = \Gamma_D \cup \Gamma_N \quad \text{with} \quad \Gamma_D \subset \partial D_D.$$

The objective function is a combination of the first eigenfrequency and of the weight of the structure

$$J(\Omega) = -\omega_1(\Omega)^2 + \ell \frac{|\Omega|}{|D|}, \tag{7.1}$$

where $\ell = 0.005$ is a fixed Lagrange multiplier for the weight constraint. The boundary conditions are displayed on Figure 7.1. Under these assumptions, the shape derivative of (7.1) is a special case of Theorem 2.5, namely

$$J'(\Omega)(\theta) = \int_{\Gamma_N} \left(\frac{\ell}{|D|} + \frac{\omega_1^2 \rho |u|^2 - Ae(u) \cdot e(u)}{\int_\Omega \rho |u|^2 dx} \right) \theta \cdot n \, ds, \tag{7.2}$$

since $\theta \cdot n = 0$ on Γ_D. In (7.2) (ω_1^2, u) denotes the first eigencouple of (2.2).

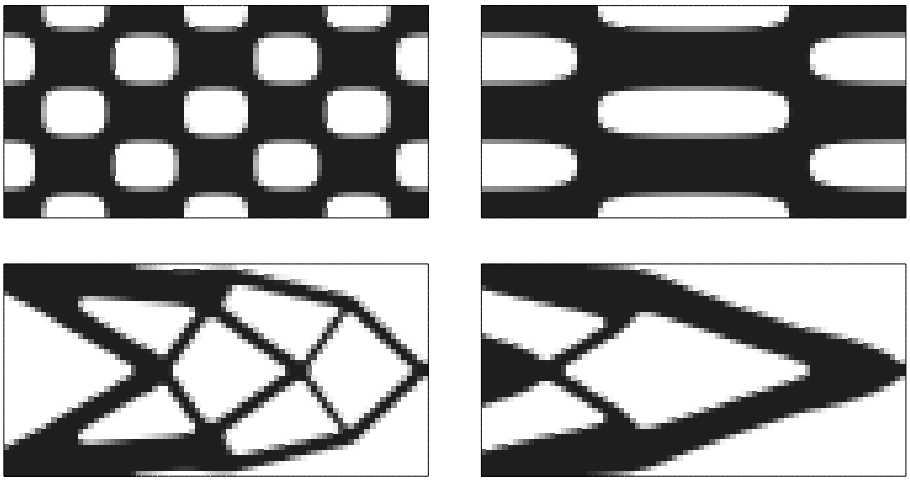

Figure 7.2: Two initializations and the resulting optimal shapes (after 50 iterations) for a 2-d cantilever

The algorithm converges smoothly to a (local) minimum which strongly depends, of course, on the initial topology as can be checked on Figures 7.2 displaying two initial configurations with a different number of holes and their optimal shapes. The optimal shapes for eigenfrequency maximization are very

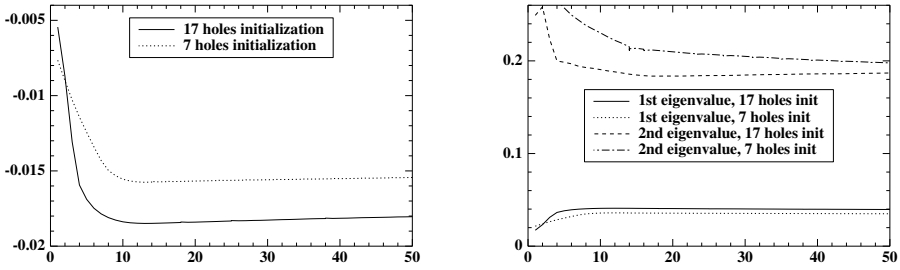

Figure 7.3: Convergence history of the objective function (left) and of the two first eigenvalues (right) for the two initializations of the 2-d cantilever of Figure 7.2

similar to those for compliance minimization (see [6]). We run 50 iterations in order to show the good convergence and stability properties of our algorithm (see Figure 7.3). The CPU cost is low since on a PC with a Pentium 4 processor (2.60GHz) this computation takes about 22 s. from which 13 s. were devoted to the 50 elasticity analysis. It is clear on Figure 7.3 (right) that the first eigenvalue always remain simple.

We run the same test case with a different size of the working domain D which is now of size 1×2 (discretized with a rectangular 80×40 mesh). Remark on Figure 7.5 (middle) that the usual two bars meeting at ninety degrees (which are optimal for compliance minimization) are complemented by a small interior cross. We also run the same test case with a lighter tip mass (of material density $\rho = 1$), see Figure 7.5 (right). One can check on Figure 7.4 that the optimal first eigenvalue is simple (the corresponding eigenmode is mostly a vertical beat). The two first eigenvalues are always clearly separated except for the heavy tip mass near the 8th iteration where a mode crossing seems to occur. At this point, the differentiability, which at the basis of the algorithm, is lost but nevertheless the eigenvalues diverge again (with no obvious reason) and the optimization can go on. Remark also that the separation of eigenvalues is definitely better in the case of a light tip mass. Therefore, we believe the role of a heavy tip mass is to produce an optimal shape which is more robust and closer to the compliance optimal shape. Once again we emphasize that for multiple eigenvalues a different algorithm should be used (see e.g. [22], [27]).

We now consider a double cantilever problem. The working domain D is of size 1.6×0.5 (discretized with a 160×50 mesh). Zero displacement boundary conditions are imposed on the left and right sides and a small square region at the center of the domain (see Figure 7.6) is 100 times heavier and is not subject to optimization.

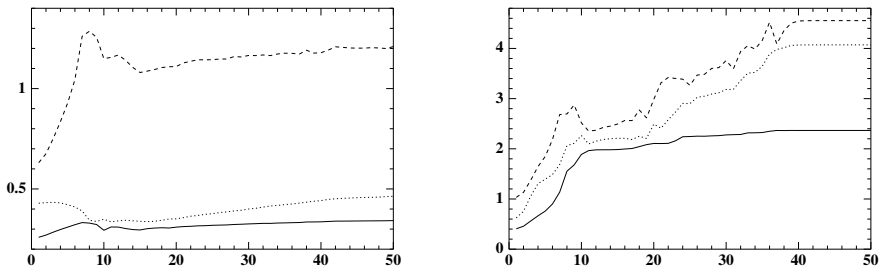

Figure 7.4: Convergence history of the three first eigenvalues for the 2-d cantilever of Figure 7.5: heavy tip mass $\rho = 100$ (left), light tip mass $\rho = 1$ (right).

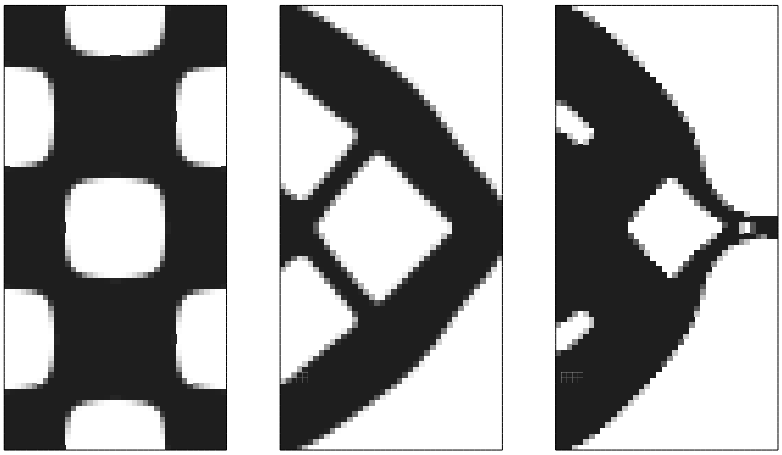

Figure 7.5: Initialization and optimal shape of a 1×2 cantilever: heavy tip mass $\rho = 100$ (middle), light tip mass $\rho = 1$ (right).

7.2 3-d cantilever

We optimize a three-dimensional cantilever. The working domain D is of size $1 \times 2 \times 1$ (discretized with a $15 \times 30 \times 15$ mesh). A zero displacement boundary condition is imposed on the left side and two cells on the middle of the right side are not subject to optimization and a material density 100 times heavier (see Figure 7.7). The objective function is still (7.1). Since the domain is not symmetric the resulting optimal shape has a simple first eigenvalue (our computations are based on this assumption). The first eigenvalue is 0.675 while the second one is 0.687.

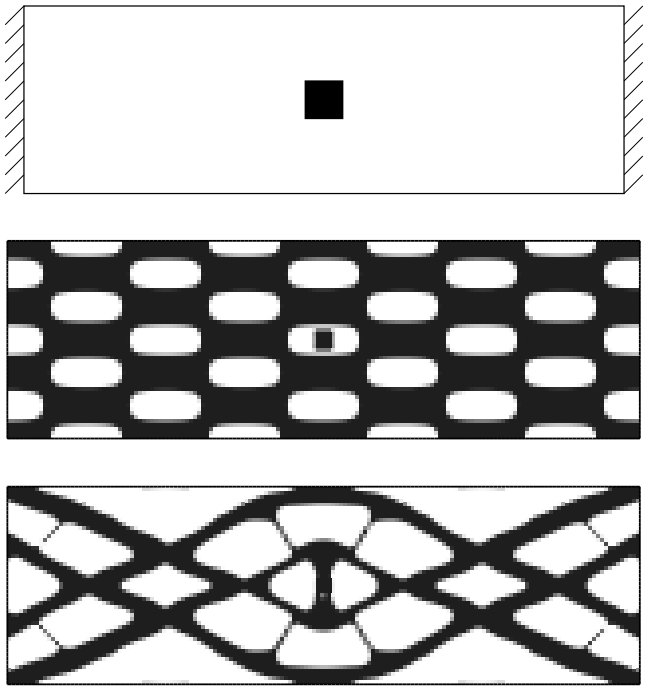

Figure 7.6: Boundary conditions, initialization and optimal shape of the double cantilever

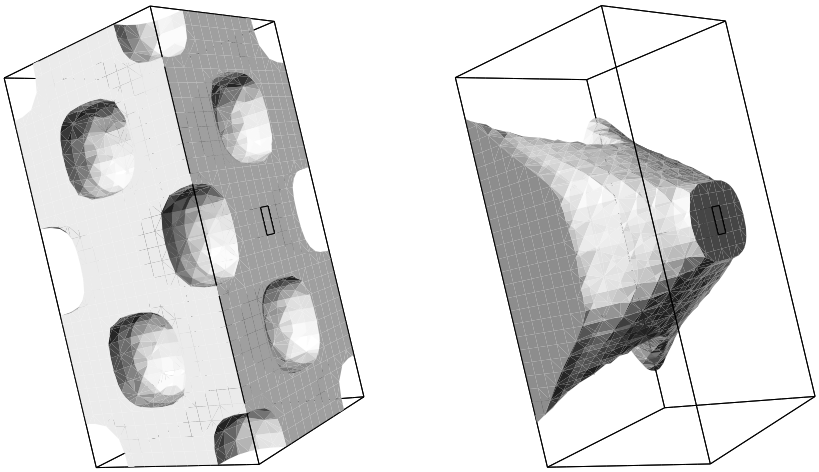

Figure 7.7: Initialization and optimal shape of a 3-d cantilever

8 Numerical results for multiple loads

For rectangular domains we use a regular quadrangular mesh with $Q1$ finite elements for the elastic displacements and an explicit second-order upwind scheme for the level-set function ψ. For general domains we use an unstructured quadrangular mesh with $Q1$ finite elements for u and an explicit first-order upwind scheme for ψ. The Young modulus E of material A is normalized to 1 and the Poisson ratio ν is fixed to 0.3. The void or holes are mimicked by an ersatz material with the same Poisson ratio and a smaller Young modulus by a factor of 10^{-3}. For each elasticity analysis (or iteration) we perform 20 (in 2-d) or 50 (in 3-d) explicit time steps of the upwind scheme for the Hamilton-Jacobi transport equation. We also reinitialize the level-set function every 5 time steps of transport by performing 5 explicit time steps of equation (4.4).

8.1 2-d bridge

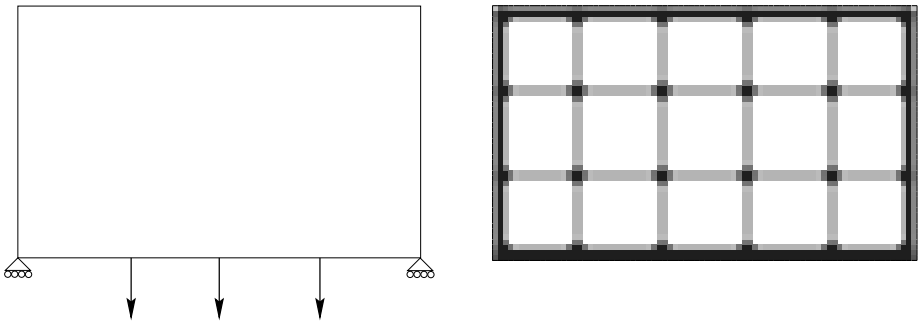

Figure 8.1: Boundary conditions and initialization of the bridge problem.

The first example in dimension $d = 2$ is a bridge problem. The working domain is a rectangle of size 2×1.2 discretized with a rectangular 80×48 mesh, at the two lower corners the vertical displacement is zero, and three unit identical vertical forces are applied at positions $x = 0.5, 1.0, 1.5$ of the bottom side (see Figure 8.1). We again impose that the shape Dirichlet boundary Γ_D is a subset of the fixed boundary ∂D_D, and the three surface loads g_i are applied at fixed points on the boundary ∂D_N. There is no body forces, i.e. $f_i \equiv 0$. This is a three loadings case and the objective function is the sum of the weight and of the three compliances

$$J(\Omega) = \ell \int_\Omega dx + \sum_{i=1}^{n} \left(\int_{\Gamma_N} g_i \cdot u_i \, ds \right).$$

According to Theorem 3.1 its shape derivative is

$$J'(\Omega)(\theta) = \int_{\Gamma_N} \left(\ell - \sum_{i=1}^{n} Ae(u_i) \cdot e(u_i) \right) \theta \cdot n \, ds.$$

For this problem we update the value of the Lagrange multiplier in order to reach a volume constraint of 20%, i.e. $|\Omega| = 0.2|D|$. At each explicit time step of the transport equation we compute the volume $|\Omega|$ and accordingly we modify ℓ for the next iteration in order to converge to the right volume constraint (see Figure 8.3). Since the volume constraint is very small, we need to change our usual initialization (used in the previous examples): the new one, displayed on Figure 8.1, satisfies the prescribed weight. The optimal design is displayed in Figure 8.2 (right). To make a clear comparison we perform a single load compliance minimization with the same parameters but with the three forces applied at the same time. The resulting single load optimal shape is also displayed on Figure 8.2 (left). One can clearly check that the multiple loads solution is much more stable than the single load solution.

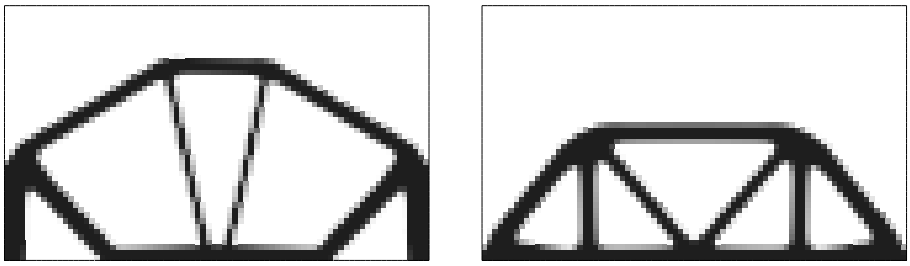

Figure 8.2: Optimal shapes of the two-dimensional bridge initialized as in Figure 8.1: single load case (left), multiple loads case (right)

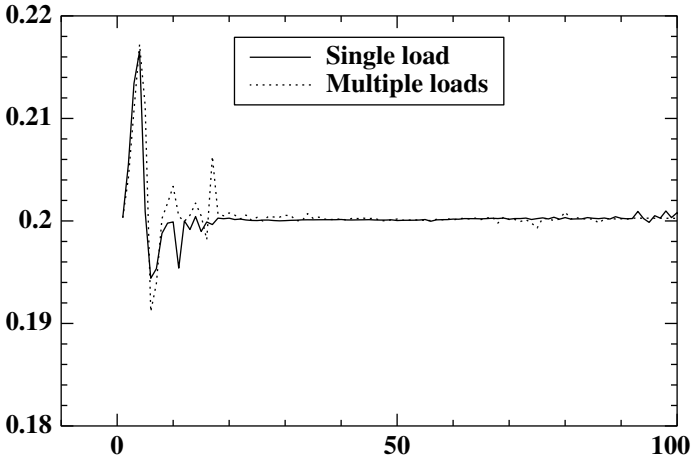

Figure 8.3: Convergence history of the weight for the bridges of Figure 8.2

8.2 Suspension triangles

We now test our method on an industrial example proposed by Peugeot and already discussed in [3]: a suspension triangle. Figure 8.4 shows the working domain, its unstructured mesh (mostly made of quadrangles but with a few triangles), the boundary conditions and the two external forces. Each load is applied separately and corresponds to different situations of driving (breaking and accelerating). The intensity of the horizontal force is 8 times larger than that of the vertical force. The three disks (at each extremity and at the corner of the part) are not subject to optimization and are made of a stiffer material (with Young modulus 80 times larger). The middle of the corner disk is fixed while one point in the upper left part of the upper disk is fixed, only in the horizontal direction. The loads are applied at the middle the lower right disk. For such a non-structured mesh the transport Hamilton-Jacobi equation (4.2) is solved by the explicit first order upwind scheme of Abgrall [1].

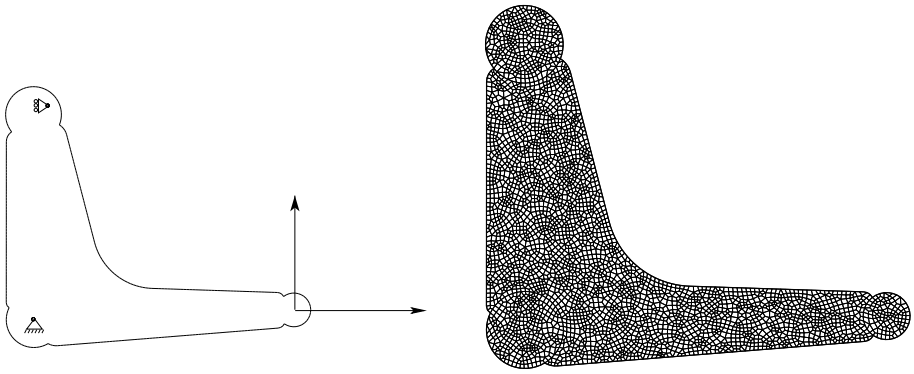

Figure 8.4: Boundary conditions and unstructured mesh of the suspension triangle.

According to the initial design the multiple loads optimization yields the shapes drawn on Figure 8.5. The resulting design is very sensitive to the initialization, even more in the multiple load case than for single load compliance optimization. As can be checked on Figure 8.6 the best design is obtained with the initialization of Figure 8.5 (right), which is not obvious to guess a priori.

8.3 3-d chairs

Multiple loads optimization works also in 3-d. We now design an optimal chair submitted to two different loads (see Figure 8.7). The four bottom corners of the design domain are fixed, while the back and the seat of the chair are not subject to optimization and support the loads. We first compute a single load

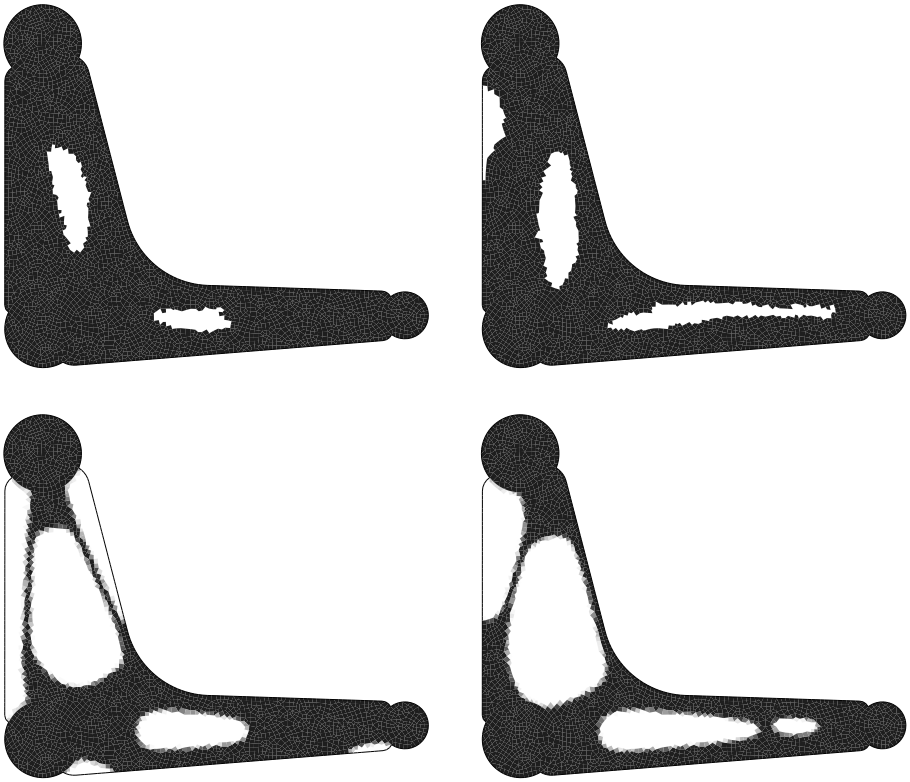

Figure 8.5: Two initializations (top) and the resulting optimal shapes (bottom) of the suspension triangle

optimal chair, i.e. the two loads are applied together (see Figure 8.8 left). The multiple loads optimal chair has a more complex topology and is more stable to load variations (see Figure 8.8 right). Both chairs have the same weight. The CPU cost is very low: on a PC with a Pentium 4 processor (2.60GHz) this computation takes about 2980 s. from which 2667 s. were devoted to the 100 elasticity analysis. A direct solver (Cholesky method) was used for solving the linear system. Remark that there is no noticeable difference of CPU time between the single or multiple loads problems since we use a direct solver (adding more loads amounts to add more backward and forward substitutions which are negligible compared to the Cholesky factorization).

8.4 3-d bridges

Finally, we compute optimal 3-d bridges. The design domain is made of a non-optimizable roadway and two lateral vertical boxes where reinforcement structures can be designed. There are 11 loading configurations corresponding

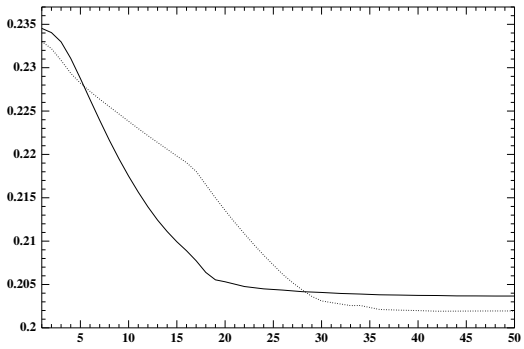

Figure 8.6: Convergence history of the objective function for the two initializations of the suspension triangle of Figure 8.5: plain line (left), dotted line (right)

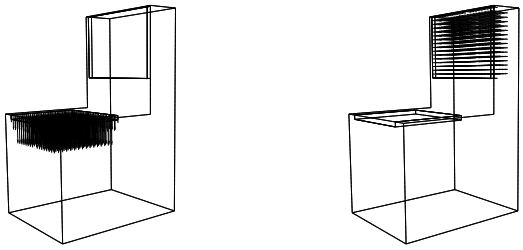

Figure 8.7: Two loading configurations for a chair

to a heavy vehicle moving across the bridge. Again we first perform a single load optimization with the 11 loads applied once at all (see Figure 8.9 left). Like in 2-d the multiple loads optimal bridge is very different and much more stable than its single load counterpart (see Figure 8.9 right). They both have the same weight.

9 Conclusion

The level set method can perform shape and topology optimization in two and three space dimensions. Its main advantages are its ability to handle drastic topology changes, its moderate cost in terms of CPU time (since it captures a shape on an Eulerian mesh), its versatility in taking into account any type of objective functions or mechanical models. As a matter of fact, with a good initialization it is as efficient as the homogenization method (when the latter one is available).

Since at each iteration we require the objective function to decrease, the main

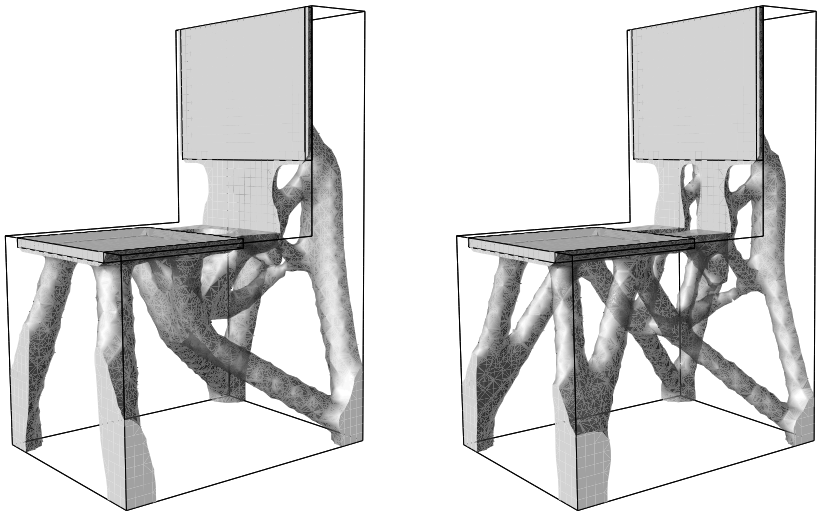

Figure 8.8: Optimal chair for the single load configuration (left) and for the multiple loads configuration (right)

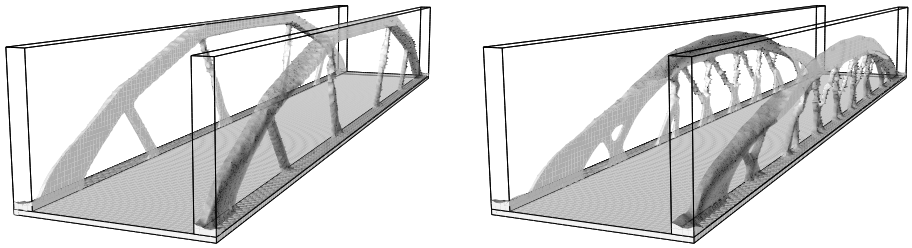

Figure 8.9: Optimal bridge for the single load configuration (left) and for the multiple loads configuration (right)

drawback of our level set method is the possibility of falling into a local (and non-global) minima if the initialization is too far from a global minimum. This is a consequence of the fact that the level-set method is not a relaxation method (unlike the homogenization method [2], [10], [18]), and thus local minima are not fully eliminated in favor of global minima. Actually the existence of local minima has been rigorously proved in 2-d by Chambolle [15] since he proved that, for any fixed maximal number of holes N, there exists an optimal shape within the class of shapes with fewer holes than N (and we know in some instances that increasing N strictly decreases the objective function). Therefore, local minima can not be avoided (at least in 2-d) by any gradient numerical method based on shape differentiation. Of course, numerical methods which

do not mandatorily decrease the objective function (like simulated annealing or any stochastic algorithms) can escape from local minima at the price of a higher computational cost. In numerical practice, the level-set method behaves differently in 2-d and 3-d. In 2-d the number of holes can decrease (by holes merging) but not increase (there is no nucleation mechanism in our algorithm). Therefore, a good initialization must contain a large number of holes if a non-trivial optimal topology is expected. In 3-d, because there is more topological freedom, new holes can easily be created (for example by crossing two separate zero level-set surfaces without breaking the connectivity of the shape or of the void).

To find an adequate initialization, one can first run the homogenization method on a simplified problem (say, linear elasticity with compliance objective function) as a pre-processor in order to find a correct initial topology. Another possibility (which is under current investigation ; see also [14] in the context of inverse problems) it to couple the level-set method with the so-called bubble method, or topological derivative, proposed by [19], [21], and [34], which yields a criteria for hole nucleation.

References

[1] Abgrall R., Numerical discretization of the first-order Hamilton-Jacobi equation on triangular meshes, *Com. Pure Applied Math.* **XLIX**, 1339-1373 (1996).

[2] Allaire G., *Shape optimization by the homogenization method, Springer Verlag, New York* (2001).

[3] G. Allaire, Z. Belhachmi, F. Jouve, The homogenization method for topology and shape optimization. Single and multiple loads case, *Revue Européenne des Eléments Finis*, **5**, 649-672 (1996).

[4] Allaire G., Bonnetier E., Francfort G., Jouve F., Shape optimization by the homogenization method. *Nümerische Mathematik* **76**, 27-68 (1997).

[5] Allaire G., Jouve F., Toader A.-M., A level-set method for shape optimization, *C. R. Acad. Sci. Paris, Série I*, **334**, 1125-1130 (2002).

[6] Allaire G., Jouve F., Toader A.-M., Structural optimization using sensitivity analysis and a level-set method, *J. Comp. Phys.*, Vol 194/1, pp.363-393 (2004).

[7] Allaire G., Kohn R.V., Optimal design for minimum weight and compliance in plane stress using extremal microstructures. *Europ. J. Mech. A/Solids* **12**, 6, 839-878 (1993).

[8] Almgren, F., Taylor, J., Optimal geometry in equilibrium and growth. Symposium in Honor of Benoit Mandelbrot (Curaçao, 1995). *Fractals* **3**, 713-723 (1995).

[9] Ambrosio L., Buttazzo G., An optimal design problem with perimeter penalization, *Calc. Var.* **1**, 55-69 (1993).

[10] Bendsoe M., *Methods for optimization of structural topology, shape and material,* Springer Verlag, New York (1995).

[11] Bendsoe M., Kikuchi N., Generating Optimal Topologies in Structural Design Using a Homogenization Method. *Comp. Meth. Appl. Mech. Eng.* **71**, 197-224 (1988).

[12] Bendsoe M., Sigmund O., *Topology Optimization. Theory, Methods, and Applications*, Springer Verlag, New York (2003).

[13] Burger M., A framework for the construction of level set methods for shape optimization and reconstruction, *Interfaces and Free Boundaries* **5**, 301-329 (2003).

[14] Burger M., Hackl B., Ring W., Incorporating topological derivatives into level set methods, *J. Comp. Phys.*, to appear.

[15] Chambolle A., A density result in two-dimensional linearized elasticity and applications. *Arch. Ration. Mech. Anal.* **167**, 211-233 (2003).

[16] Céa J., Conception optimale ou identification de formes, calcul rapide de la dérivée directionnelle de la fonction coût, *Math. Model. Num. Anal.* **20**, 3, 371-402 (1986).

[17] Chenais D., On the existence of a solution in a domain identification problem, *J. Math. Anal. Appl.* **52**, 189-289 (1975).

[18] Cherkaev A., *Variational Methods for Structural Optimization,* Springer Verlag, New York (2000).

[19] Eschenauer H., Schumacher A., Bubble method for topology and shape optimization of structures, *Structural Optimization*, **8**, 42-51 (1994).

[20] Folgado J., Rodrigues H. , Structural optimization with a non-smooth buckling load criterion, *Control and Cybernetics* **27**, 235-253 (1998).

[21] Garreau S., Guillaume P., Masmoudi M., The topological asymptotic for PDE systems: the elasticity case. *SIAM J. Control Optim.* **39**, no. 6, 1756-1778 (2001).

[22] Haug E., Rousselet B., Design sensitivity analysis in structural mechanics. II. Eigenvalue variations, *J. Struct. Mech.* **8**, 161-186 (1980).

[23] Kane C., Schoenauer M., Topological optimum design using genetic algorithms, *Control and Cybernetics*, **25**, 1059-1088 (1996).

[24] Mohammadi B., Pironneau O., *Applied shape optimization for fluids,* Clarendon Press, Oxford (2001).

[25] Murat F., Simon S., Etudes de problèmes d'optimal design. *Lecture Notes in Computer Science 41, 54-62, Springer Verlag, Berlin* (1976).

[26] Neves M., Rodrigues H., Guedes J., Generalized topology design of structures with a buckling load criterion, *Struct. Optim.* **10**, 71-78 (1995).

[27] Olhoff N., Seyranian A.P., Lund E., Multiple eigenvalues in structural optimization problems, *Struct. Optim.* **8**, 207-227 (1994).

[28] Osher S., Santosa F., level-set methods for optimization problems involving geometry and constraints: frequencies of a two-density inhomogeneous drum. *J. Comp. Phys.*, **171**, 272-288 (2001).

[29] Osher S., Sethian J.A., Front propagating with curvature dependent speed: algorithms based on Hamilton-Jacobi formulations. *J. Comp. Phys.* **78**, 12-49 (1988).

[30] Pironneau O., *Optimal shape design for elliptic systems, Springer-Verlag, New York,* (1984).

[31] Sethian J.A., *Level-Set Methods and fast marching methods: evolving interfaces in computational geometry, fluid mechanics, computer vision and materials science,* Cambridge University Press (1999).

[32] Sethian J., Wiegmann A., Structural boundary design via level-set and immersed interface methods. *J. Comp. Phys.,* **163**, 489-528 (2000).

[33] Simon J., Differentiation with respect to the domain in boundary value problems. *Num. Funct. Anal. Optimz.*, **2**, 649-687 (1980).

[34] Sokołowski J., Żochowski A., Topological derivatives of shape functionals for elasticity systems. *Mech. Structures Mach.* **29**, no. 3, 331-349 (2001).

[35] Sokołowski J., Zolesio J.P., *Introduction to shape optimization: shape sensitivity analysis, Springer Series in Computational Mathematics, Vol. 10, Springer, Berlin,* (1992).

[36] Wang M.Y., Wang X., Guo D., A level-set method for structural topology optimization, *Comput. Methods Appl. Mech. Engrg.*, **192**, 227-246 (2003).

[37] Wang M.Y., Wang X., Guo D., Structural shape and topology optimization in a level set based implicit moving boundary framework, *preprint.*